Measuring the dark matter content of dwarf spheroidal galaxies

Vulcano Workshop 2022 — Frontier Objects in Astrophysics and Particle Physics (Elba Island, 2022/09/25-10/01)

FRANCESCO G. SATURNI (INAF-OAR & ASI-SSDC)
for the CTA Consortium

Colls.: L. A. Antonelli, M. Doro, S. Lombardi, A. Morselli, K. D. Nakashima, G. Rodríguez-Fernández

Outline

- The quest for DM in the Universe
- Main targets for indirect searches of heavy DM
- Measuring DM densities in dSph halos
- Summary

The quest for dark matter in the Universe

— The DM content of the Universe
— The zoo of particle DM candidates
— Direct vs indirect DM detection
— The expected γ-ray flux from DM self-interaction

The quest for DM in the universe

Dark matter (DM) is the major component of the Universe's matter content:

1. ~22% of the total Universe's energy budget;
2. ~85% of the Universe's matter content.

Its existence is only indirectly inferred so far from several astrophysical/cosmological observations.

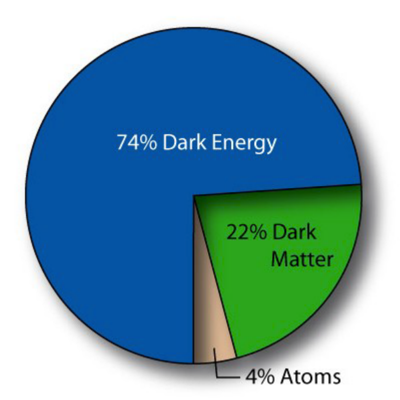

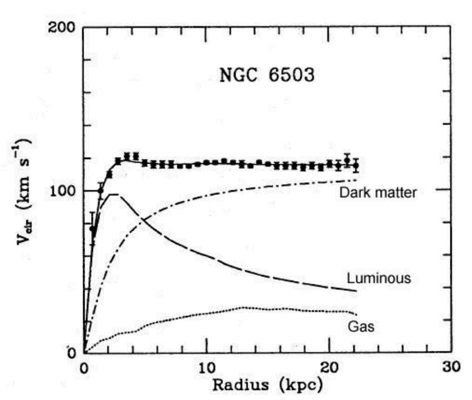

Rotation curves of galaxies

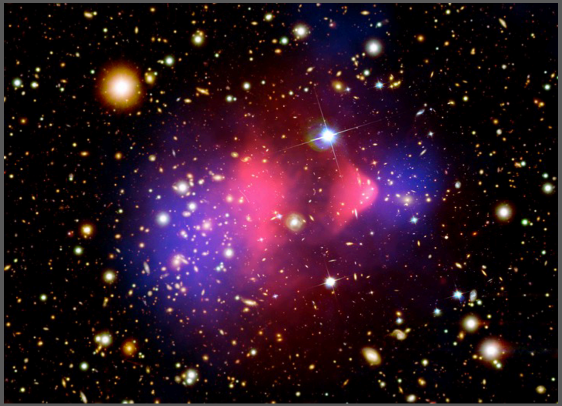

Peculiar objects (e.g. Bullet Cluster)

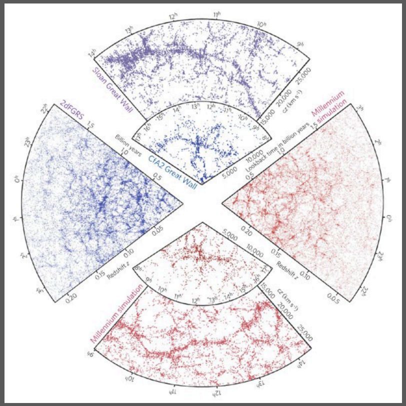

Cosmological large-scale structures

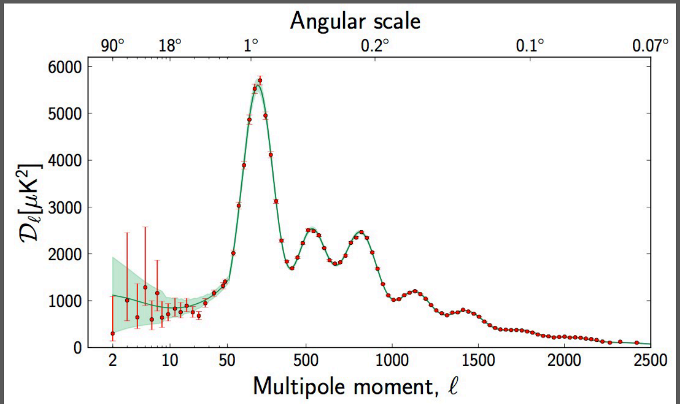

CMB oscillations

See M. Vecchi's talk!

The quest for DM in the universe

The zoo of particle DM theories:

1. spread over 48 orders of magnitude in mass and >50 in interaction cross section;
2. origin of DM components from corruptions in the spacetime quantum structure to remnants of primordial macroscopic objects.

Current preferred paradigm: DM is composed by particles belonging to the WIMP (weakly interacting massive particles) family.

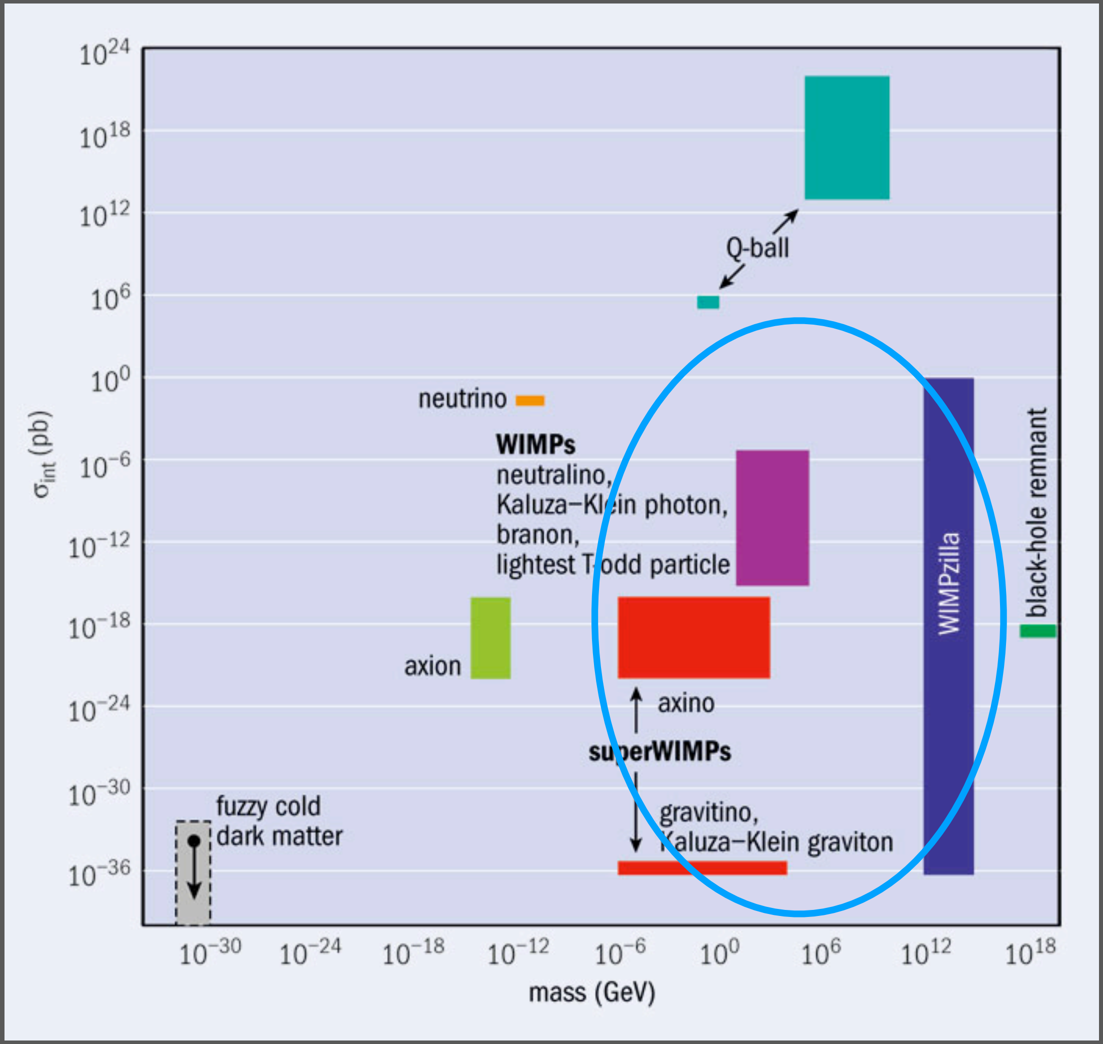

See M. Vecchi's talk!

The quest for DM in the universe

Events of dark-baryonic matter interaction never observed so far:

1. DM cross section for interaction with baryonic matter must be extremely small (order of weak interactions or below)

Production of DM candidates in particle accelerators never achieved so far:

2. DM production must be a rare process that happens only in extreme conditions (e.g. the primordial Universe)

<u>Indirect detection</u> to look for production of Standard Model (SM) particles from DM self-interaction.

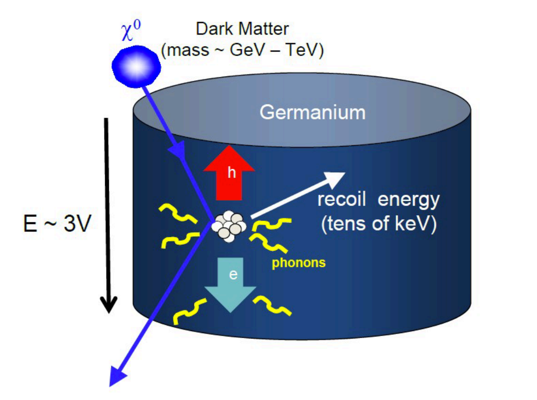

Direct detection (collision with baryonic matter)

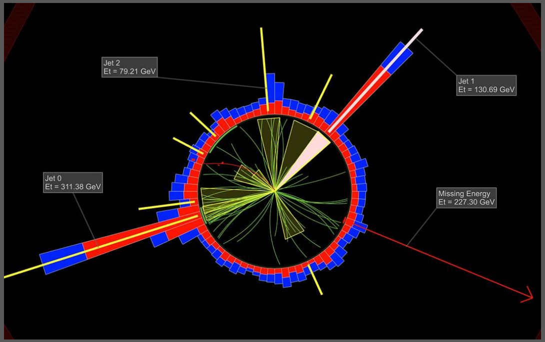

Direct detection (production in particle accelerators)

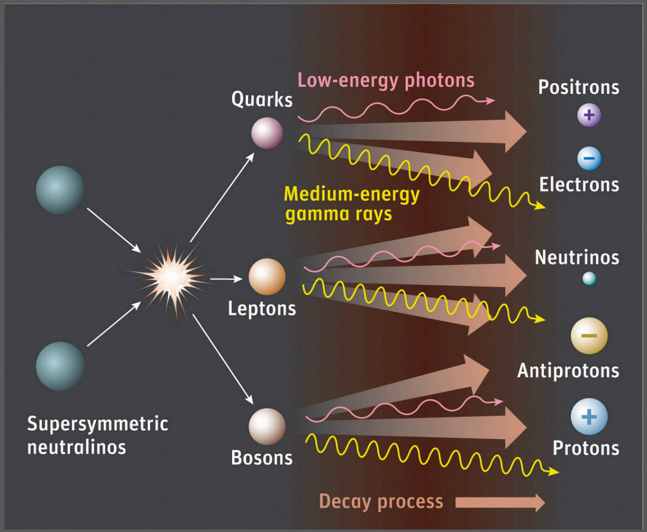

Indirect detection (self-interaction into SM products)

See M. Vecchi's talk!

The quest for DM in the universe

See M. Vecchi's talk!

Expected γ-ray flux from WIMP self-interaction decomposed into:

1. particle-physics term (flux for single interactions);
2. astrophysical term — the so-called J-factor (for annihilation) or D-factor (for decay).

$$J(\Delta\Omega) = \int_{\Delta\Omega} d\Omega \int_{\mathrm{l.o.s.}} \rho^2_{\mathrm{DM}}(\ell;\Omega) d\ell$$

$$D(\Delta\Omega) = \int_{\Delta\Omega} d\Omega \int_{\mathrm{l.o.s.}} \rho_{\mathrm{DM}}(\ell;\Omega) d\ell$$

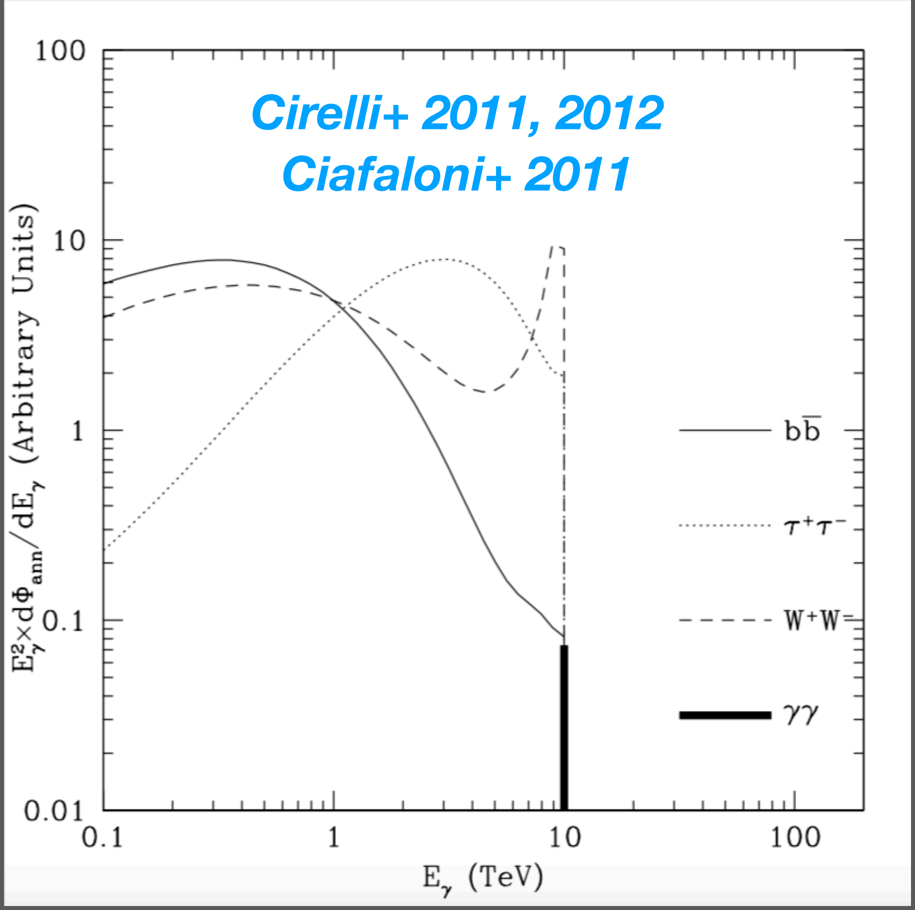

Spectral shapes expected for DM self-interaction into SM pairs

Main targets for indirect searches of heavy dark matter

— The dwarf spheroidal galaxies
— Prospects for new discoveries

Main targets for heavy DM searches

Milky Way center & ridge (very close, but highly bog-contaminated and with uncertain DM profile)

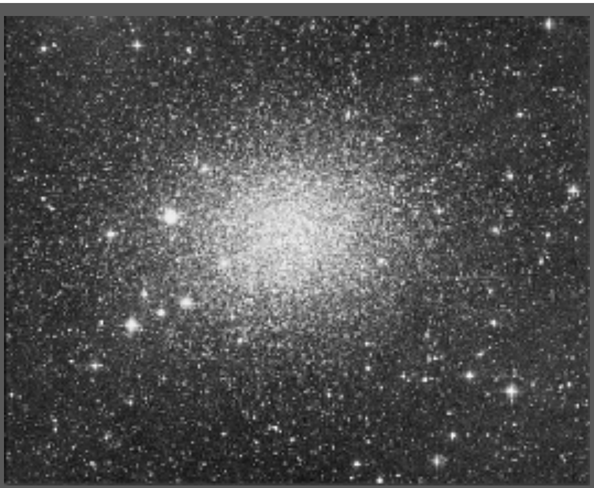

Dwarf spheroidal galaxies (high M/L ratio and no bkg, but small halos => intrinsically low DM content)

Galaxy clusters (high DM content, but far and possibly bkg-contaminated)

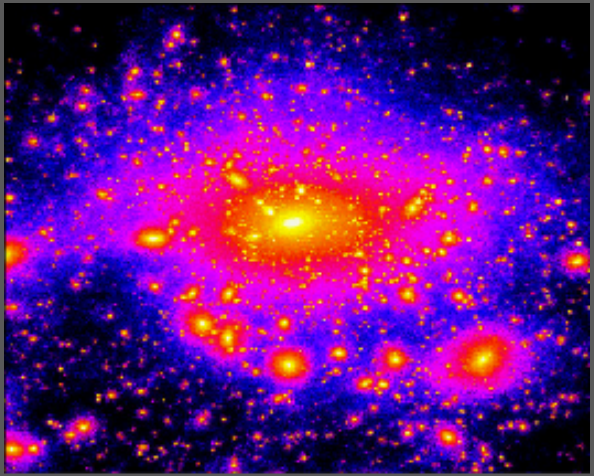

Dark clumps (galaxies without stars, only theoretically predicted so far

Main targets for heavy DM searches

Dwarf spheroidal galaxies (dSphs) are satellites of the Milky Way and other Local Group galaxies that exhibit virial masses much higher than what expected from their stellar luminosities (McConnachie 2012).

Possible reason: **extreme DM domination**.

The Sculptor dSph (credits: D. Malin, AAO)

virial theorem $2\langle \mathscr{T} \rangle + \langle U \rangle = 0$

vel. dispersion $3 m_* \sigma_r^2 = \dfrac{G M_{\rm tot} m_*}{R}$

gravitational mass $M_{\rm tot} = \dfrac{3 R \sigma_r^2}{G}$

$$m_* \approx 1\,\mathbf{M}_\odot \rightarrow M_* \approx N\,\mathbf{M}_\odot \Rightarrow L_{\rm tot} \approx N\,\mathbf{L}_\odot$$

expected

$$\left(\frac{M_{\rm tot}}{L_{\rm tot}}\right)_{\rm theo} = \frac{M_*}{L_{\rm tot}} \approx 1$$

measured

$$10 \lesssim \left(\frac{M_{\rm tot}}{L_{\rm tot}}\right)_{\rm meas} \lesssim 1000$$

Main targets for heavy DM searches

Several dSphs known around the MW.

Two main categories:

1. classical dSphs — O(100) to O(1000) member stars
2. ultra-faint dSphs — less than O(10) to less than O(100) member stars

Many more (ultra-faint) dSphs are being discovered now thanks to performance improvements of telescope technologies.

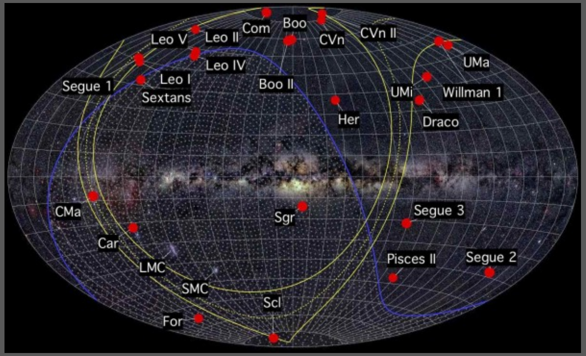

Sky distribution of dSphs

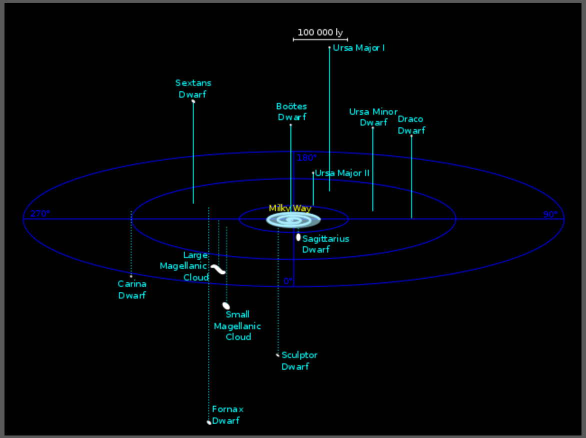

3D distribution of dSphs

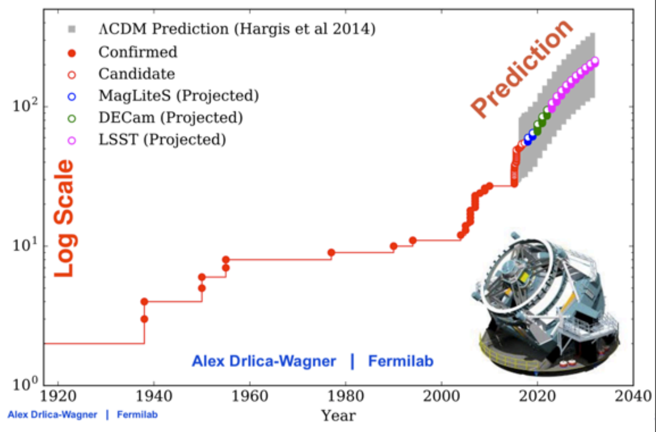

Prospects for future discoveries of dSphs cherenkov telescope array

Measuring dark matter densities in dwarf galaxy halos

— The Jeans analysis
— The sample selection
— Input priors and assumptions
— The astrophysical factors of dSph halos
— Caveats in the analysis

Measuring DM densities in dSph halos

DM was introduced to explain the velocity distribution of galaxies in the Coma cluster (Zwicky 1930) and later adopted to successfully describe the flattening of rotation curves in spiral galaxies (Zwicky 1933, Bertone & Hooper 2016).

Rotation curves of spiral galaxies usually derived from measurements of gas clouds; for other types of galaxies, problems are:

1. no or little rotational support;
2. no gas to measure rotation velocity.

Need of a paradigm change (equations + velocity tracer):

JEANS ANALYSIS

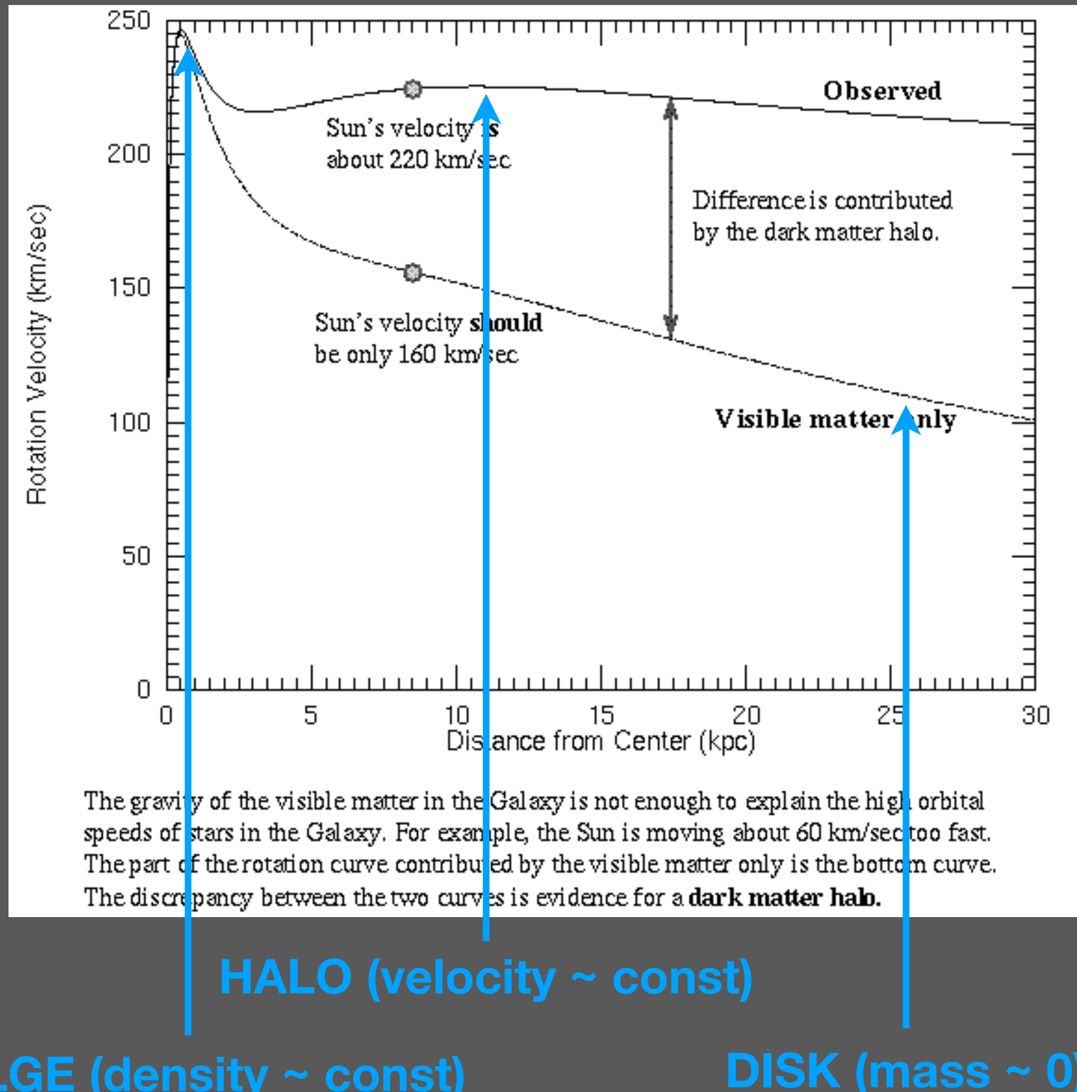

The gravity of the visible matter in the Galaxy is not enough to explain the high orbital speeds of stars in the Galaxy. For example, the Sun is moving about 60 km/sec too fast. The part of the rotation curve contributed by the visible matter only is the bottom curve. The discrepancy between the two curves is evidence for a **dark matter halo.**

Measuring DM densities in dSph halos

- Jeans analysis assumptions:
  - Collisionless system
  - Steady state
  - Negligible rotational support
  - Spherical symmetry (not essential)

- Second-order development of the Jeans equations (Binney & Tremaine 2008):

$$\frac{1}{n_*}\left[\frac{d}{dr}\left(n_*\overline{v_r^2}\right)\right]+\frac{2}{r}\beta_{\mathrm{ani}}(r)\overline{v_r^2}=-\frac{G\left[M_{\mathrm{DM}}(r)+M_*(r)\right]}{r^2}$$

$$n_* = n_*(r)$$

luminosity profiles

$$\beta_{\mathrm{ani}}(r) = 1-\frac{\overline{v_\theta^2}}{\overline{v_r^2}}$$

velocity anisotropy

$$M_*(r) \approx 0$$

DM domination (if verified)

Measuring DM densities in dSph halos

The Jeans analysis of dSph kinematics is one of the methods that provides the most robust constraints on the DM amount in such halos.

Example: **MCMC Jeans analysis of dSph kinematics with CLUMPY** (Charbonnier+ 2012, Bonnivard+ 2016, Hütten+ 2019).

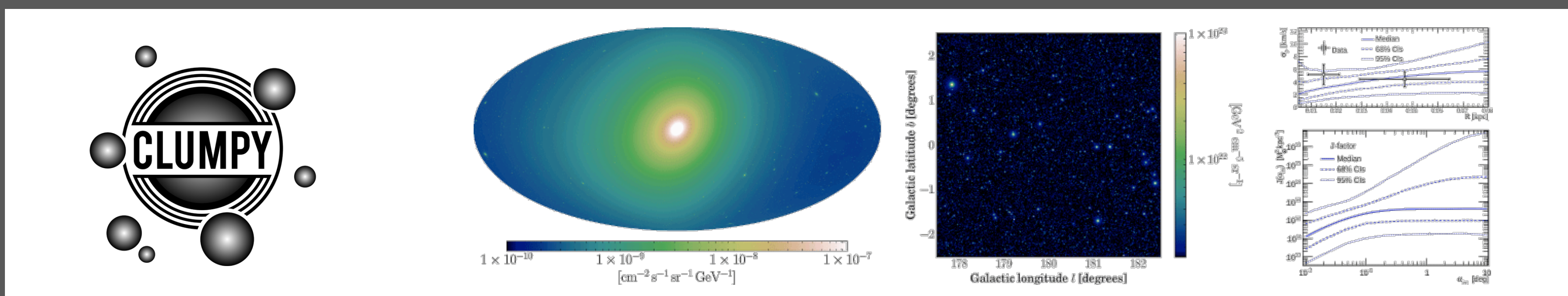

Alternatives:

- Empyrical models of the dSph stellar velocity dispersion (Evans+ 2004)
- Likelihood maximization of the Jeans equation (Strigari+ 2008, Geringer-Sameth+ 2015, Hayashi+ 2016)
- Semi-analytical J-factor integration (Acciari+ 2010, Evans+ 2016)
- Bayesian analysis of halo properties (Martínez+ 2011)

Measuring DM densities in dSph halos

Optimal dSphs selected according to:

1. Distance ($d < 100$ pc)
2. Culmination zenith angle ($ZA_{min} < 30°$)

Targets with no/poor brightness and/or kinematic data excluded from the MCMC Jeans analysis.

Surviving sample:

— 6 Northern dSphs (1 classical + 5 ultra-faint)

— 6 Southern dSphs (3 classical + 3 ultra-faint)

CTA Cons. 2022 (in prep.)

Name	Abbr.	Type	R.A. (hh mm ss)	dec. (dd mm ss)	Distance (k[illegible]c)	ZA[illegible] (deg[illegible]	ZA[illegible]	Month	[illegible]ef.
Andromeda XVIII	AndXVIII	uft	00 02 14.5	+45 05 20	1330 ± 104	16.3	69.7	Sep	McConnachie (2012); Makarova et al. (2017)
Aquarius	Aqr	uft	20 46 51.8	−12 50 53	1030 ± 57	41.6	11.8	Aug	McConnachie (2012); Ordoñez and Sarajedini (2016)
Boötes I	BoöI	uft	14 00 06.0	+14 30 00	65 ± 3	14.3	39.1	Apr	McConnachie (2012); Okamoto et al. (2012)
Boötes II	BoöII	uft	13 58 00.0	+12 51 00	39 ± 2	15.9	37.5	Apr	McConnachie (2012); Sesar et al. (2014)
Boötes III	BoöIII	uft	13 57 12.0	+26 48 00	46 ± 2	2.0	51.4	Apr	McConnachie (2012); Sesar et al. (2014)
Canes Venatici I	CVnI	uft	13 28 03.5	+33 33 21	216 ± 8	4.8	58.2	Apr	McConnachie (2012); Okamoto et al. (2012)
Canes Venatici II	CVnII	uft	12 57 10.0	+34 19 15	159 ± 8	5.6	58.9	Apr	McConnachie (2012); Okamoto et al. (2012)
Carina	Car	cls	06 41 36.7	−50 57 58	106 ± 1	79.7	26.3	Dec	McConnachie (2012); Karczmarek et al. (2015)
Cetus I	CetI	uft	00 26 11.0	−11 02 40	748 ± 31	39.8	13.6	Sep	McConnachie (2012); Dambis et al. (2013)
Cetus II	CetII	uft	01 17 52.8	−17 25 12	30 ± 3	46.2	7.2	Oct	Drlica-Wagner et al. (2015)
Columba I	ColI	uft	05 31 26.4	−28 01 48	182 ± 18	56.8	3.4	Dec	Drlica-Wagner et al. (2015)
Coma Berenices	CBe	uft	12 26 59.0	+23 54 15	42 ± 2	4.9	48.5	Mar	McConnachie (2012); Musella et al. (2009)
Draco I	DraI	cls	17 20 12.4	+57 54 55	75 ± 4	29.2	82.5	Jun	McConnachie (2012); Hernitschek et al. (2016)
Draco II	DraII	uft	15 52 47.6	+64 33 55	20 ± 3	35.8	89.2	May	Laevens et al. (2015a)
Eridanus II	EriII	uft	03 44 21.5	−43 31 48	330 ± 16	72.3	18.9	Nov	Bechtol et al. (2015)
Eridanus III	EriIII	uft	02 22 45.5	−52 16 48	95 ± 27	81.0	27.7	Oct	Bechtol et al. (2015)
Fornax	For	cls	02 39 59.3	−34 26 57	146 ± 1	63.2	9.8	Oct	McConnachie (2012); Karczmarek et al. (2015)
Grus I	GruI	uft	22 56 42.4	−50 09 48	120 ± 17	78.9	25.5	Sep	Koposov et al. (2015a)
Grus II	GruII	uft	22 04 04.8	−46 26 24	53 ± 5	75.2	21.8	Aug	Drlica-Wagner et al. (2015)
Hercules	Her	uft	16 31 02.0	+12 47 30	137 ± 11	16.0	37.4	May	McConnachie (2012); Garling et al. (2018)
Horologium I	HorI	uft	02 55 28.9	−54 06 36	87 ± 13	82.9	29.5	Oct	Bechtol et al. (2015)
Hydra II	HyaII	uft	12 21 42.1	−31 59 07	134 ± 10	60.7	7.4	Mar	Martin et al. (2015)
Indus I	IndI	uft	21 08 48.1	−51 09 36	69 ± 16	79.9	26.5	Aug	Bechtol et al. (2015)
Indus II	IndII	uft	20 38 52.8	−46 09 36	214 ± 16	74.9	21.5	Aug	Drlica-Wagner et al. (2015)
Laevens 3	Lae3	uft	21 06 54.3	+14 58 48	67 ± 3	13.8	39.6	Aug	Laevens et al. (2015a)
Leo I	LeoI	cls	10 08 28.1	+12 18 23	272 ± 10	16.5	36.9	Feb	McConnachie (2012); Stetson et al. (2014)
Leo II	LeoII	cls	11 13 28.8	+22 09 06	240 ± 9	6.6	46.8	Mar	McConnachie (2012); Tully et al. (2013)
Leo IV	LeoIV	uft	11 32 57.0	−00 32 00	151 ± 4	29.3	24.1	Mar	McConnachie (2012); Medina et al. (2018)
Leo V	LeoV	uft	11 31 09.6	+02 13 12	169 ± 5	26.5	26.9	Mar	McConnachie (2012); Medina et al. (2018)
Leo T	LeoT	uft	09 34 53.4	+17 03 05	377 ± 28	11.7	41.7	Feb	McConnachie (2012); Ripepi et al. (2014)
Phoenix I	PheI	uft	01 51 06.3	−44 26 41	427 ± 31	73.2	19.8	Oct	McConnachie (2012); Ripepi et al. (2014)
Phoenix II	PheII	uft	23 39 57.6	−54 24 36	95 ± 18	83.2	29.8	Sep	Bechtol et al. (2015)
Pictor I	PicI	uft	04 43 48.0	−50 16 48	126 ± 24	79.0	25.7	Nov	Bechtol et al. (2015)
Pisces II	PscII	uft	22 58 31.0	+05 57 09	182 ± 13	22.8	30.6	Sep	McConnachie (2012); Sand et al. (2012)
Reticulum II	RetII	uft	03 35 40.9	−54 03 00	32 ± 2	82.8	29.4	Nov	Bechtol et al. (2015)
Reticulum III	RetIII	uft	03 45 26.3	−60 27 00	92 ± 13	89.2	35.8	Nov	Drlica-Wagner et al. (2015)
Sagittarius I	SgrI	dis	18 55 19.5	−30 32 43	31 ± 1	59.3	5.9	Jul	McConnachie (2012); Valcheva et al. (2015)
Sagittarius II	SgrII	uft	19 52 40.5	−22 04 05	67 ± 5	50.8	2.6	Jul	Laevens et al. (2015a)
Sculptor	Scl	cls	01 00 09.4	−33 42 33	84 ± 2	62.5	9.1	Oct	McConnachie (2012); Martínez-Vázquez et al. (2015)
Segue 1	Seg1	uft	10 07 04.0	+16 04 55	23 ± 2	12.7	40.7	Feb	McConnachie (2012); de Jong et al. (2008)
Segue 2	Seg2	uft	02 19 16.0	+20 10 31	36 ± 2	8.6	44.8	Oct	McConnachie (2012); Boettcher et al. (2013)
Sextans	Sex	cls	10 13 03.0	−01 36 53	84 ± 3	30.4	23.0	Feb	McConnachie (2012); Medina et al. (2018)
Triangulum II	TriII	uft	02 13 17.4	+36 10 42	30 ± 2	7.4	60.8	Oct	Koposov et al. (2015a)
Tucana I	TucI	uft	22 41 49.6	−64 25 10	855 ± 35	—	39.8	Sep	McConnachie (2012); Dambis et al. (2013)
Tucana II	TucII	uft	22 52 16.7	−58 33 36	58 ± 6	87.3	33.9	Sep	Bechtol et al. (2015)
Tucana III	TucIII	uft	23 56 35.9	−59 36 00	25 ± 2	88.4	35.0	Sep	Drlica-Wagner et al. (2015)
Tucana IV	TucIV	uft	00 02 55.3	−60 51 00	48 ± 4	89.6	36.2	Sep	Drlica-Wagner et al. (2015)
Ursa Major I	UMaI	uft	10 34 52.8	+51 55 12	105 ± 2	23.2	76.6	Mar	McConnachie (2012); Brown et al. (2012)
Ursa Major II	UMaII	uft	08 51 30.0	+63 07 48	35 ± 2	34.4	87.8	Feb	McConnachie (2012); Dall'Ora et al. (2012)
Ursa Minor	UMi	cls	15 09 08.5	+67 13 21	68 ± 2	38.5	—	May	McConnachie (2012); Ruhland et al. (2011)
Willman 1	Wil1	uft	10 49 21.0	+51 03 00	38 ± 7	22.3	75.7	Mar	McConnachie (2012); de Jong et al. (2008)

Measuring DM densities in dSph halos

CLUMPY parametrization of input/output quantities:

- Empirically driven DM density profiles
  - Einasto (1965, cuspy)
  - Burkert (1995, cored)

$$\rho_{\rm DM}^{\rm Ein}(r) = \rho_s \exp\left\{-\frac{2}{\alpha}\left[\left(\frac{r}{r_s}\right)^{\alpha} - 1\right]\right\}$$

$$\rho_{\rm DM}^{\rm Bur}(r) = \frac{\rho_s}{\left(1 + r/r_s\right)\left[1 + \left(r/r_s\right)^2\right]}$$

- Light profile from surface luminosity fitting
  - 3D Zhao-Hernquist (generalized NFW)

$$\Sigma_*(R) = 2\int_R^{+\infty} \frac{n_*(r)r}{\sqrt{r^2 - R^2}}dr$$

- Most general solution for velocity anisotropy profile
  - Baes & van Hese (2007)

$$\rho_{\rm DM}(r) = \tilde{\rho}_{\rm DM}\left[\psi(r), r\right] = f(\phi)g(r) \Rightarrow \beta_{\rm ani}(r) = -\frac{1}{2}\left(\frac{d\ln g}{d\ln r}\right) = \frac{\beta_0 + \beta_\infty (r/r_a)^\eta}{1 + (r/r_a)^\eta}$$

Measuring DM densities in dSph halos

CLUMPY input data: **surface brightness profile** + kinematics of dSph member stars.

Surface brightness of dSphs fitted with 3D Zhao-Hernquist profiles projected onto 2D data.

$$n^*(r) = \frac{n_s^*}{\left(\frac{r}{r_s^*}\right)^{\gamma^*} \left[1 + \left(\frac{r}{r_s^*}\right)^{\alpha^*}\right]^{\frac{\beta^* - \gamma^*}{\alpha^*}}}$$

Name	Site	M_V (mag)	ϵ	ρ_s^* (10^5 $L_\odot$ kpc^{-3})	r_s^* (kpc)	α^*	β^*	γ^*	Ref.	Membership	N_{mem}	$\langle v_r \rangle$ km s^{-1}	σ_v km s^{-1}	Ref.
BoöI	N	-6.3 ± 0.2	0.39 ± 0.06	1.14 ± 0.21	0.461 ± 0.021	1.1	7.7	0.0	[1,2]	bin	37	100.6	4.3	[12]
CBe	N	-4.1 ± 0.5	0.38 ± 0.14	1.08 ± 0.50	0.0740 ± 0.0035	1.1	5.4	0.0	[1,3]	bin	59	97.8	5.8	[13]
DraI	N	-8.8 ± 0.3	0.31 ± 0.02	4.5 ± 1.3	0.1473 ± 0.0079	6.8	3.8	0.0	[1,4]	EM	466	−292.4	9.5	[14]
GruII	S	-3.9 ± 0.2	~0.2	1.58 ± 0.29	0.166 ± 0.016	1.3	7.6	0.0	[5]	bin	21	−109.8	1.8	[15]
RetII	S	-3.6 ± 0.2	0.6 ± 0.2	2.04 ± 0.19	0.0408 ± 0.0026	3.5	4.7	1.1	[6]	bin	18	64.0	3.6	[16]
Scl	S	-11.1 ± 0.5	0.32 ± 0.03	23 ± 11	0.2100 ± 0.0050	3.2	4.0	0.6	[1,4]	EM	1120	111.5	9.1	[17]
Seg1	N	-1.5 ± 0.8	0.48 ± 0.13	1.21 ± 0.89	0.0739 ± 0.0064	1.1	9.2	0.2	[1,7]	EM	154	206	15	[18]
Sex	S	-9.3 ± 0.5	0.35 ± 0.05	0.56 ± 0.26	0.493 ± 0.018	2.7	4.0	0.6	[1,4]	EM	356	224	11	[17]
SgrI	S	-13.5 ± 0.3	0.64 ± 0.02	0.277 ± 0.076	1.869 ± 0.060	1.1	4.9	0.0	[1,8]	EM	288	140	17	[19]
SgrII	S	-5.2 ± 0.4	~0.2	42.9 ± 3.9	0.0371 ± 0.0028	3.5	5.7	0.1	[9,10]	bin	21	−175.7	5.0	[20]
TriII	N	-1.8 ± 0.5	~0.2	7.3 ± 3.4	0.0342 ± 0.0023	1.2	5.3	0.0	[11]	bin	13	−381.7	2.5	[21]
Wil1	N	-2.7 ± 0.8	0.47 ± 0.08	4.4 ± 3.3	0.0251 ± 0.0046	1.2	5.9	0.0	[1,7]	bin	40	−13.6	6.3	[22]

CTA Cons. 2022 (in prep.)

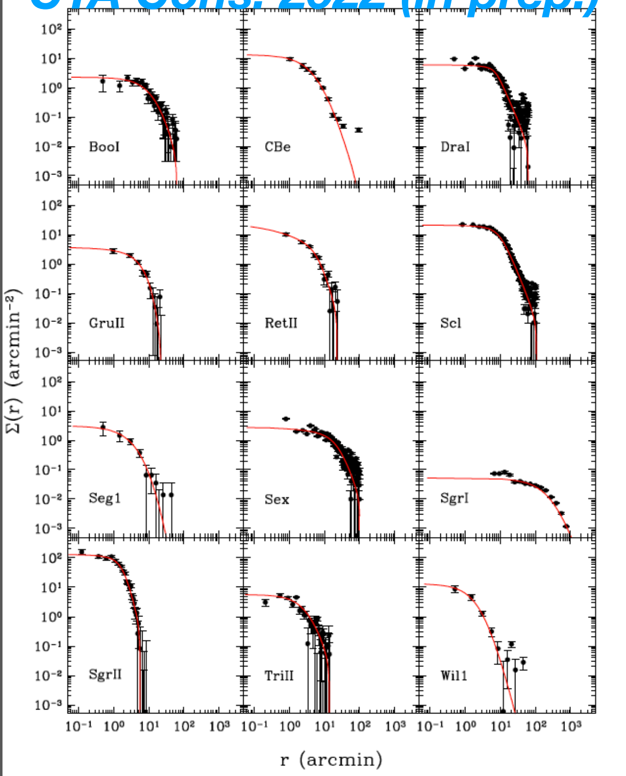

Measuring DM densities in dSph halos

CLUMPY input data: surface brightness profile + **kinematics of dSph member stars**.

Stellar memberships estimated through an EM algorithm (Walker+ 2009) with a cut at 95% CL (classical + Seg1) or adopted as binary (0/1, ultrafaint).

$$p_{\rm mem}\left(v_i, W_i\right) = \frac{\exp\left\{-\frac{1}{2}\left[\frac{\left(v_i - \langle v_{\rm mem}\rangle\right)^2}{\sigma(v)^2_{\rm mem} + \sigma(v)^2_i} + \frac{\left(W_i - \langle W_{\rm mem}\rangle\right)^2}{\sigma(W)^2_{\rm mem} + \sigma(W)^2_i}\right]\right\}}{2\pi\sqrt{\left[\sigma(v)^2_{\rm mem} + \sigma(v)^2_i\right]\left[\sigma(W)^2_{\rm mem} + \sigma(W)^2_i\right]}}$$

$$p_{\rm Bes}\left(v_i\right) = \frac{1}{N_{\rm Bes}\sigma_{\rm Bes}\sqrt{2\pi}}\sum_{i=1}^{N_{\rm Bes}}\exp\left\{-\frac{\left[v^{(i)}_{\rm Bes} - v_i\right]^2}{2\sigma^2_{\rm Bes}}\right\}$$

$$p_{\rm non}\left(v_i, W_i\right) = \frac{p_{\rm Bes}\left(v_i\right)}{\sqrt{2\pi\left[\sigma(W)^2_{\rm non} + \sigma(W)^2_i\right]}}\exp\left\{-\frac{\left(W_i - \langle W_{\rm non}\rangle\right)^2}{2\left[\sigma(W)^2_{\rm non} + \sigma(W)^2_i\right]}\right\}$$

Name	Site	M_V (mag)	ϵ	ρ^*_s (10^5 L$_\odot$ kpc^{-3})	r^*_s (kpc)	α^*	β^*	γ^*	Ref.	Membership	$N_{\rm mem}$	$\langle v_r\rangle$ km s^{-1}	σ_v km s^{-1}	Ref.
BoöI	N	-6.3 ± 0.2	0.39 ± 0.06	1.14 ± 0.21	0.461 ± 0.021	1.1	7.7	0.0	[1,2]	bin	37	100.6	4.3	[12]
CBe	N	-4.1 ± 0.5	0.38 ± 0.14	1.08 ± 0.50	0.0740 ± 0.0035	1.1	5.4	0.0	[1,3]	bin	59	97.8	5.8	[13]
DraI	N	-8.8 ± 0.3	0.31 ± 0.02	4.5 ± 1.3	0.1473 ± 0.0079	6.8	3.8	0.0	[1,4]	EM	466	−292.4	9.5	[14]
GruII	S	-3.9 ± 0.2	~0.2	1.58 ± 0.29	0.166 ± 0.016	1.3	7.6	0.0	[5]	bin	21	−109.8	1.8	[15]
RetII	S	-3.6 ± 0.2	0.6 ± 0.2	2.04 ± 0.19	0.0408 ± 0.0026	3.5	4.7	1.1	[6]	bin	18	64.0	3.6	[16]
Scl	S	-11.1 ± 0.5	0.32 ± 0.03	23 ± 11	0.2100 ± 0.0050	3.2	4.0	0.6	[1,4]	EM	1120	111.5	9.1	[17]
Seg1	N	-1.5 ± 0.8	0.48 ± 0.13	1.21 ± 0.89	0.0739 ± 0.0064	1.1	9.2	0.2	[1,7]	EM	154	206	15	[18]
Sex	S	-9.3 ± 0.5	0.35 ± 0.05	0.56 ± 0.26	0.493 ± 0.018	2.7	4.0	0.6	[1,4]	EM	356	224	11	[17]
SgrI	S	-13.5 ± 0.3	0.64 ± 0.02	0.277 ± 0.076	1.869 ± 0.060	1.1	4.9	0.0	[1,8]	EM	288	140	17	[19]
SgrII	S	-5.2 ± 0.4	~0.2	42.9 ± 3.9	0.0371 ± 0.0028	3.5	5.7	0.1	[9,10	bin	21	−175.7	5.0	[20]
TriII	N	-1.8 ± 0.5	~0.2	7.3 ± 3.4	0.0342 ± 0.0023	1.2	5.3	0.0	[11]	bin	13	−381.7	2.5	[21]
Wil1	N	-2.7 ± 0.8	0.47 ± 0.08	4.4 ± 3.3	0.0251 ± 0.0046	1.2	5.9	0.0	[1,7]	bin	40	−13.6	6.3	[22]

CTA Cons. 2022 (in prep.)

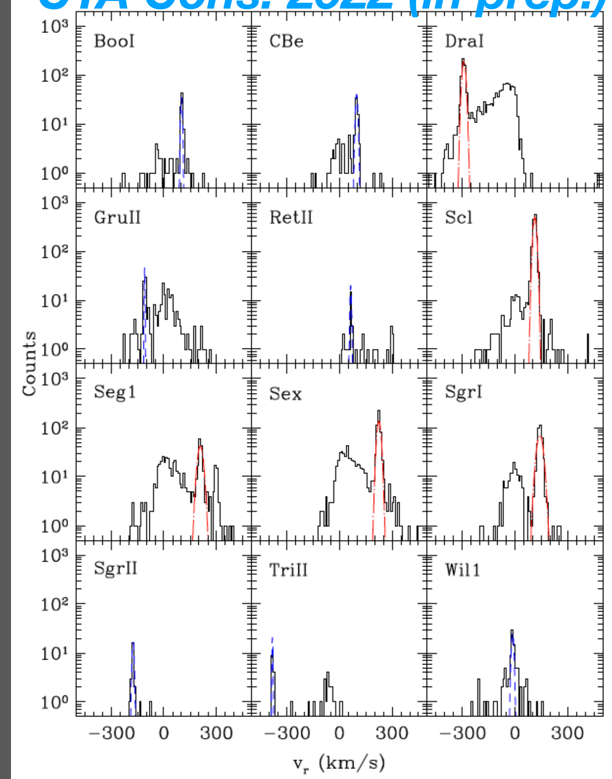

Measuring DM densities in dSph halos

DM density profiles computed from posterior distributions of best-fit parameters.

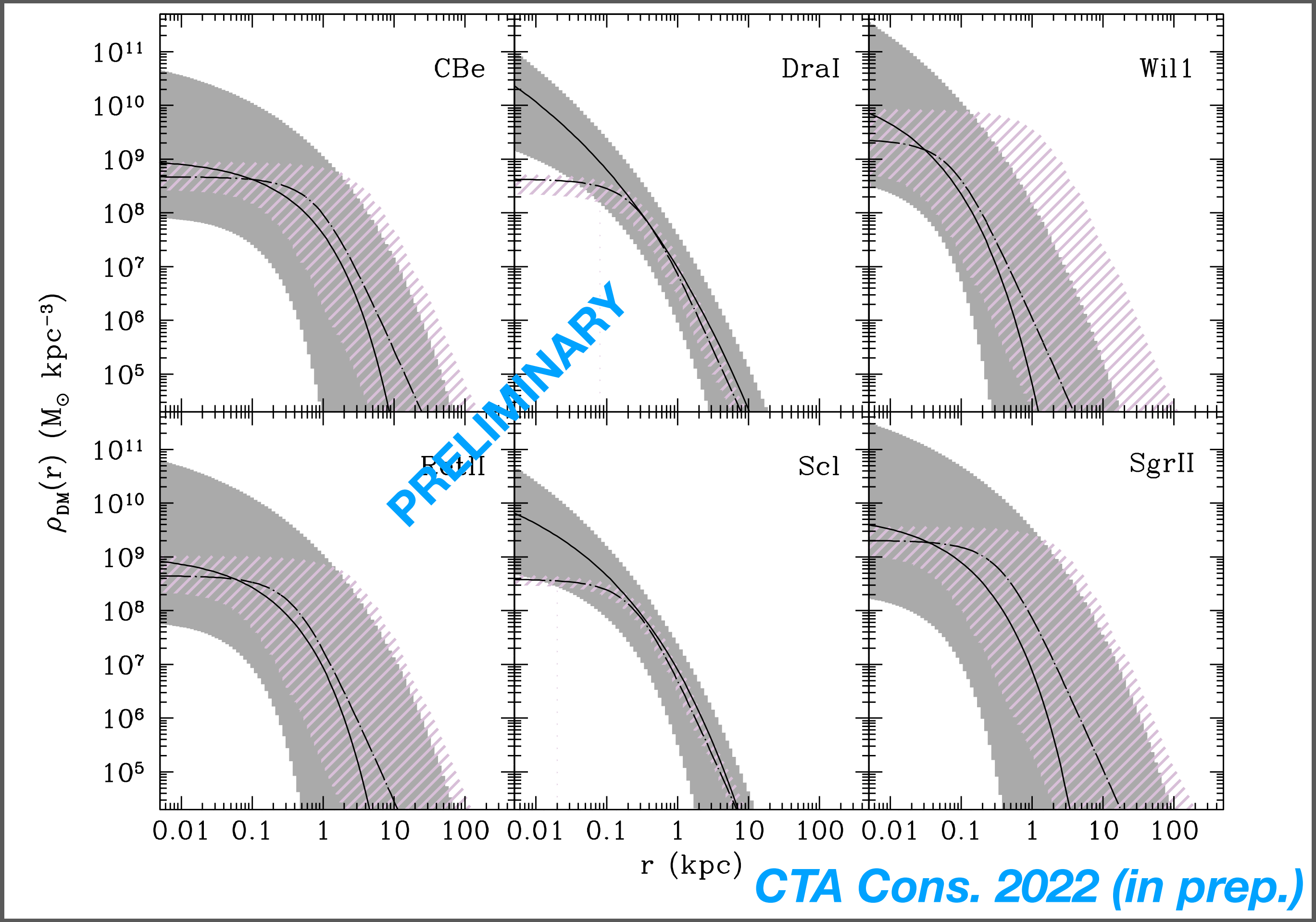

Measuring DM densities in dSph halos

Astrophysical factors (Einasto profile) for DM annihilation and decay computed from posterior distributions of best-fit parameters as a function of the integration angle.

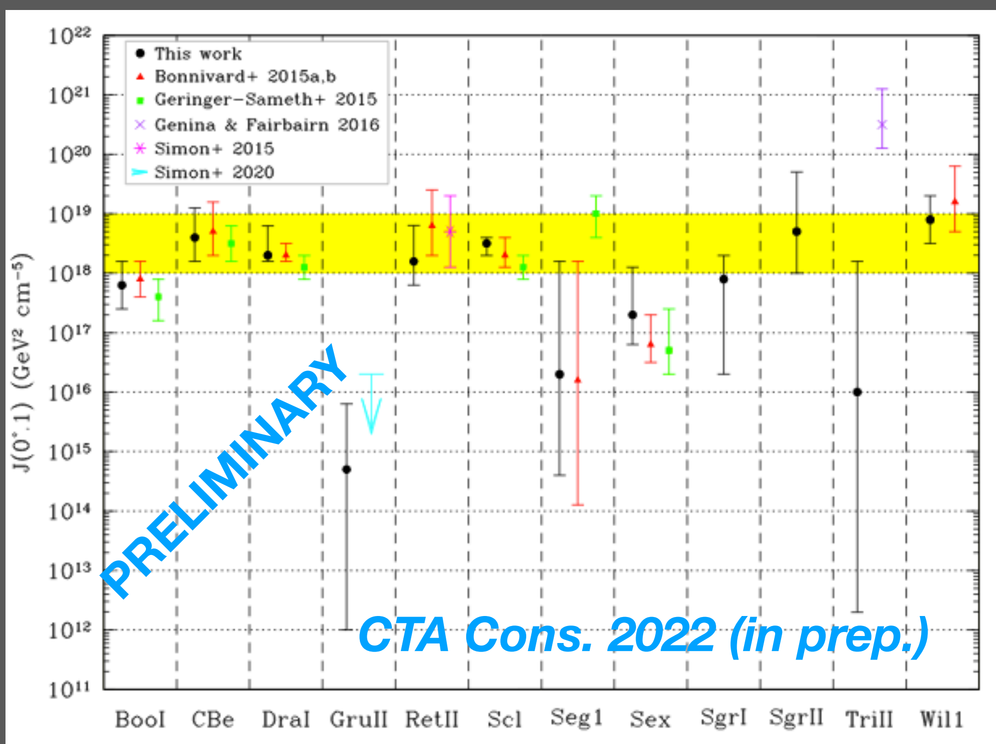

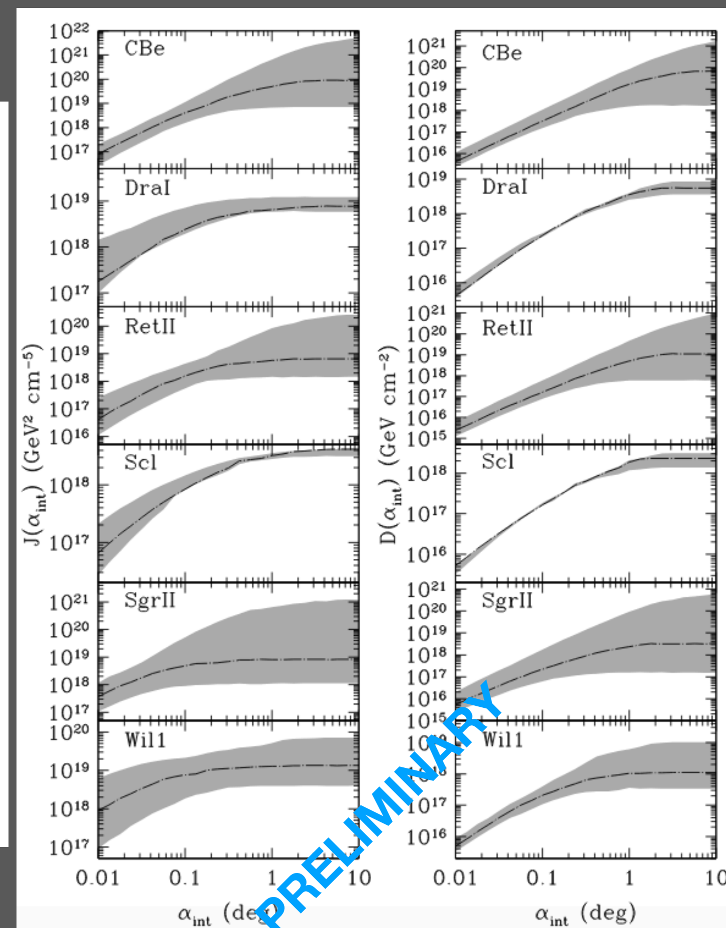

Measuring DM densities in dSph halos

Scaling relations for the astrophysical factors as a function of the dSph distance.

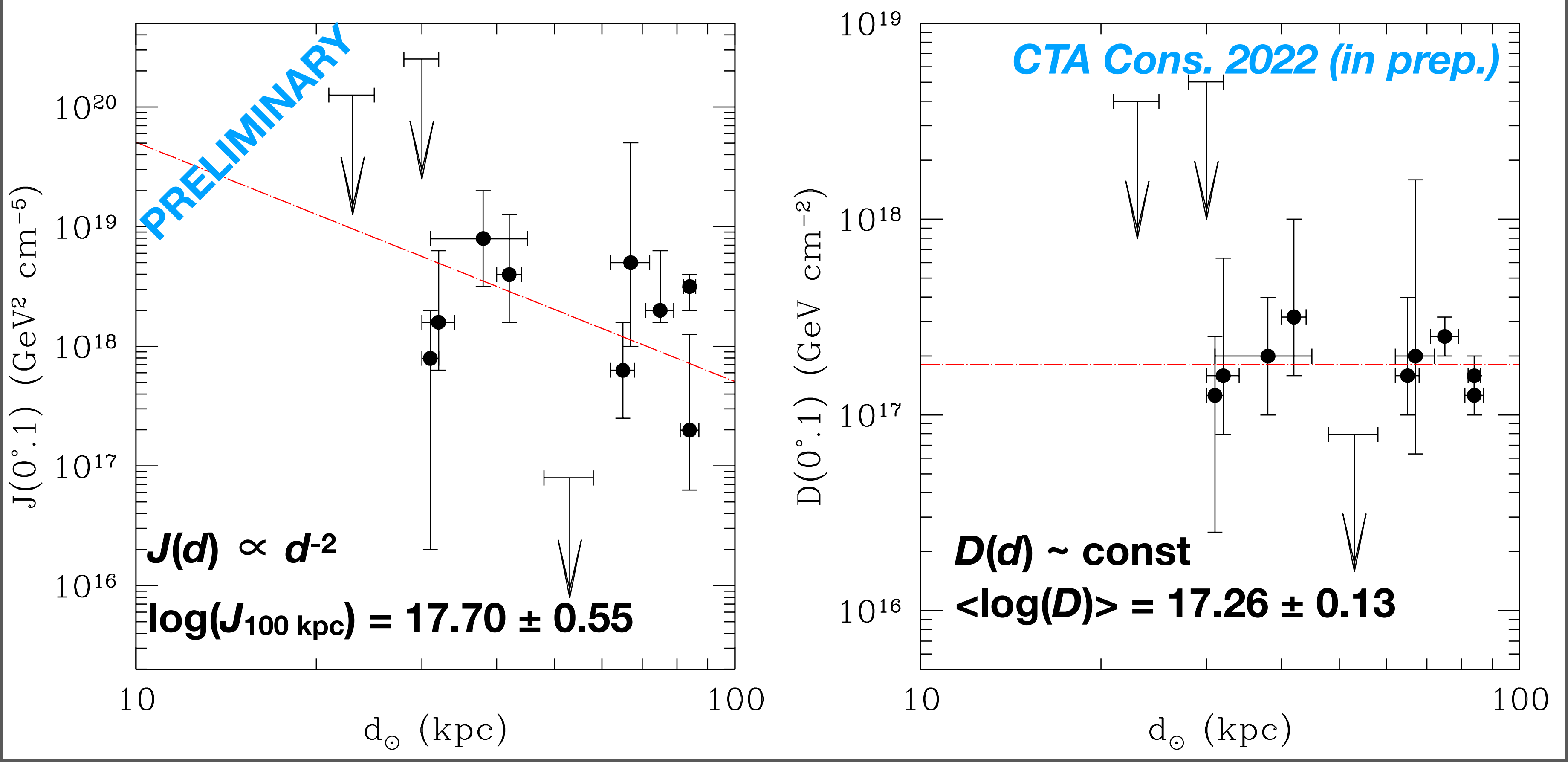

Summary

— Conclusions
— Future work

Summary

Conclusions

- Indirect DM searches are a hot topic in modern astrophysics.
  - Constraining DM parameters (particle mass, cross section, decay time)
  - Inferring the physical conditions of the primordial Universe
- Reliable determination of the precise amount and distribution of DM in halos around astrophysical sources is of paramount importance.
  - Need of developing robust techniques dedicated to such an issue
  - Need of targeting robust objects (MW center, dSphs, galaxy clusters)
- DM density profiles of dSph halos can be computed from MCMC Jeans analysis on their confirmed member stars.
  - Calculation of astrophysical factors for DM self-interaction processes
  - Selection of best targets for indirect DM searches
  - Derivation of scaling relations with target distance

Summary

Future work

- X-check the MCMC Jeans analysis of dSph halos with results from other set-ups and techniques.

- Improvement of the MCMC technique.
  - Treatment of the brightness profile as a set of free parameters
  - Improvement of the membership estimation for dSph stars

- Discovery of new targets and knowledge improvement of the existing ones.
  - New dSphs from more sensitive sky surveys
  - Increase of the stellar samples available for the ultra-faint targets

Thank you!

Supplementary material

— Build-up of the expected γ-ray flux from DM self-interaction
— Robustness of the astrophysical DM reservoirs
— Expected density profiles in DM halos
— Mathematical derivation of the Jeans equation
— Caveats on the determination of astrophysical factors

Supplementary material

- WIMP pair annihilation into SM pairs (Bergström+ 1998):

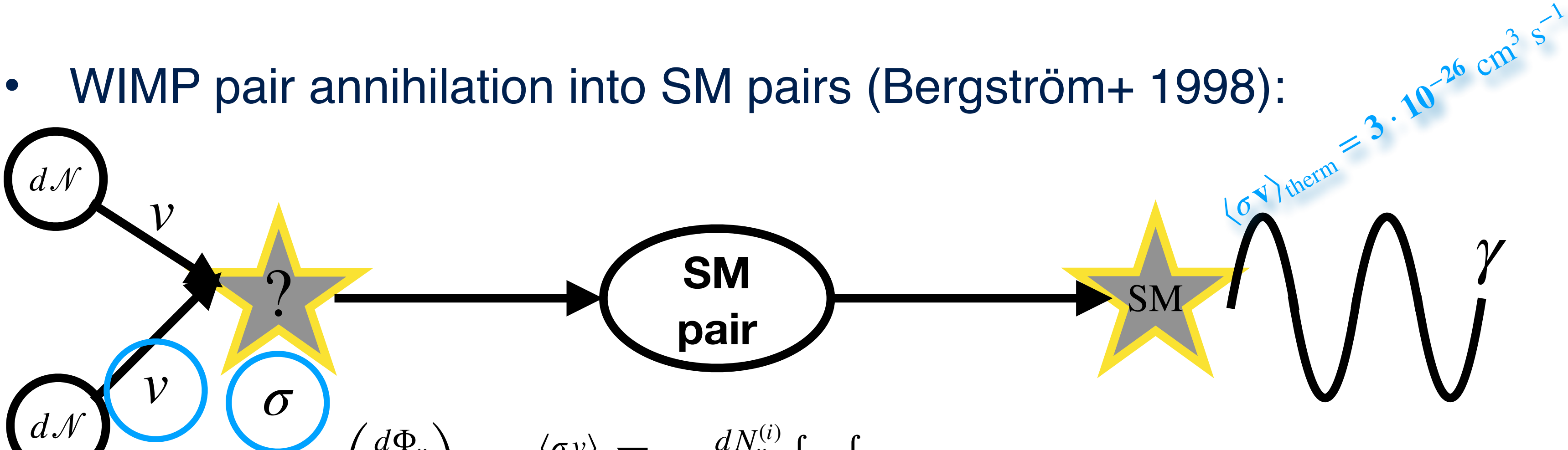

$$\left(\frac{d\Phi_\gamma}{dE_\gamma}\right)_{\text{ann}} = \frac{\langle \sigma v \rangle}{8\pi m_\chi^2} \sum_i \text{BR}_i \frac{dN_\gamma^{(i)}}{dE_\gamma} \int_{\Delta\Omega} \int_{\text{l.o.s.}} \rho_{\text{DM}}^2(\ell, \Omega) d\ell d\Omega$$

- WIMP particle decay into SM pairs:

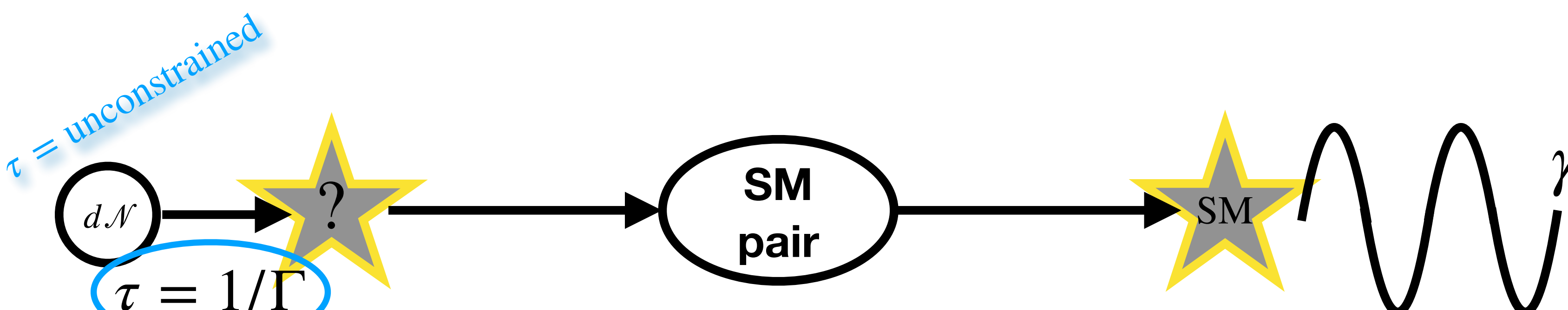

$$\left(\frac{d\Phi_\gamma}{dE_\gamma}\right)_{\text{dec}} = \frac{1}{4\pi m_\chi} \sum_i \Gamma_i \frac{dN_\gamma^{(i)}}{dE_\gamma} \int_{\Delta\Omega} \int_{\text{l.o.s.}} \rho_{\text{DM}}(\ell, \Omega) d\ell d\Omega$$

Supplementary material

Building up the expected γ-ray flux from DM self-interaction (e.g., annihilation):

- Differential photon number produced in 1 annihilation event

$$f_\gamma^{(i)} = \mathrm{BR}_i \frac{dN_\gamma^{(i)}}{dE_\gamma}$$

- Probability of impact for 2 DM particles

$$\frac{d\mathcal{N} \times d\mathcal{N}}{2} = \frac{1}{2} n^2(\ell;\Omega)\sigma_{\mathrm{ann}} v\,dt\,d\mathcal{V} = \frac{\rho_{\mathrm{DM}}^2(\ell;\Omega)}{2m_\chi^2}\sigma_{\mathrm{ann}} v\,dt\,d\mathcal{V}$$

- Differential flux for elementary volumes

$$\frac{(d\mathcal{N})^2/2}{4\pi d_\oplus^2 dt} \times \sum_i f_\gamma^{(i)} = \frac{\sigma_{\mathrm{ann}} v}{8\pi m_\chi^2} \times \sum_i \mathrm{BR}_i \frac{dN_\gamma^{(i)}}{dE_\gamma} \times \frac{\rho_{\mathrm{DM}}^2(\ell;\Omega)}{d_\oplus^2} d\mathcal{V}$$

- Integration over volume and velocity average

$$\frac{d\Phi_{\mathrm{ann}}}{dE_\gamma} = \frac{\langle \sigma_{\mathrm{ann}} v \rangle}{8\pi m_\chi^2} \sum_i \mathrm{BR}_i \frac{dN_\gamma^{(i)}}{dE_\gamma} J(\Delta\Omega)$$

Supplementary material

Signal intensity vs. detection robustness of the known/supposed DM reservoirs:

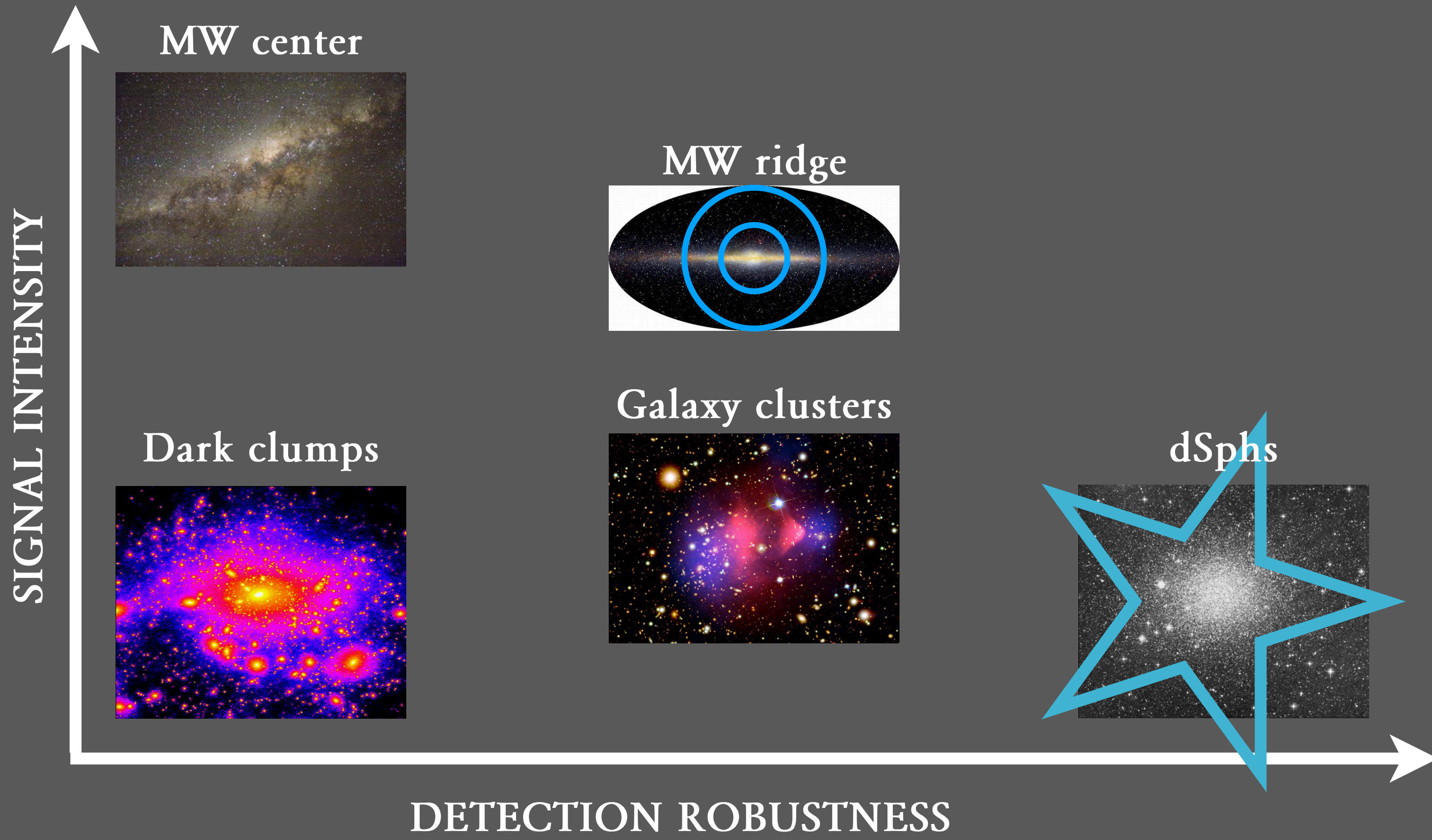

Supplementary material

Elementary derivation of the kinematics in a DM halo:

BULGE

$$\rho(r) = \textbf{const} = \rho_0$$

$$\nabla^2\Phi = \frac{1}{r^2}\left[\frac{d}{dr}\left(r^2\frac{d\Phi}{dr}\right)\right] = -4\pi G\rho_0$$

$$\cancel{r^2}\frac{d\Phi}{dr} - \cancel{r^2\frac{d\Phi}{dr}}\Big|_{r=0} = -\frac{4}{3}\pi G\rho_0 r^3$$

$$v(r) = 2r\sqrt{\frac{\pi}{3}G\rho_0} \propto r$$

DISK

$$M(r) \approx \textbf{const} = M_{\text{bulge}}$$

$$\Phi(r) = \frac{GM_{\text{bulge}}}{r}$$

$$r\frac{d\Phi}{dr} = -\frac{GM_{\text{bulge}}}{r}$$

$$v(r) = \sqrt{\frac{GM_{\text{bulge}}}{r}} \propto r^{-1/2}$$

HALO

$$v(r) \approx \textbf{const} = v_\infty$$

$$\Phi(r) = \Phi_s - v_\infty^2 \ln\left(\frac{r}{r_s}\right)$$

$$r\frac{d\Phi}{dr} = -v_\infty^2$$

$$\frac{1}{r^2}\left[\frac{d}{dr}\left(r^2\frac{d\Phi}{dr}\right)\right] = -\left(\frac{v_\infty}{r}\right)^2 = -4\pi G\rho(r)$$

$$\rho(r) = \frac{v_\infty^2}{4\pi G r^2} \propto r^{-2}$$

Supplementary material

DM density profiles proposed in the literature to explain the rotation curve features found in observations and cosmological simulations:

1. Einasto (1965, cuspy to cored)
2. Zhao (1996) & Hernquist (1990, cuspy to cored)
3. Burkert (1995, cored)
4. Navarro, Frenk & White (1996, cuspy)

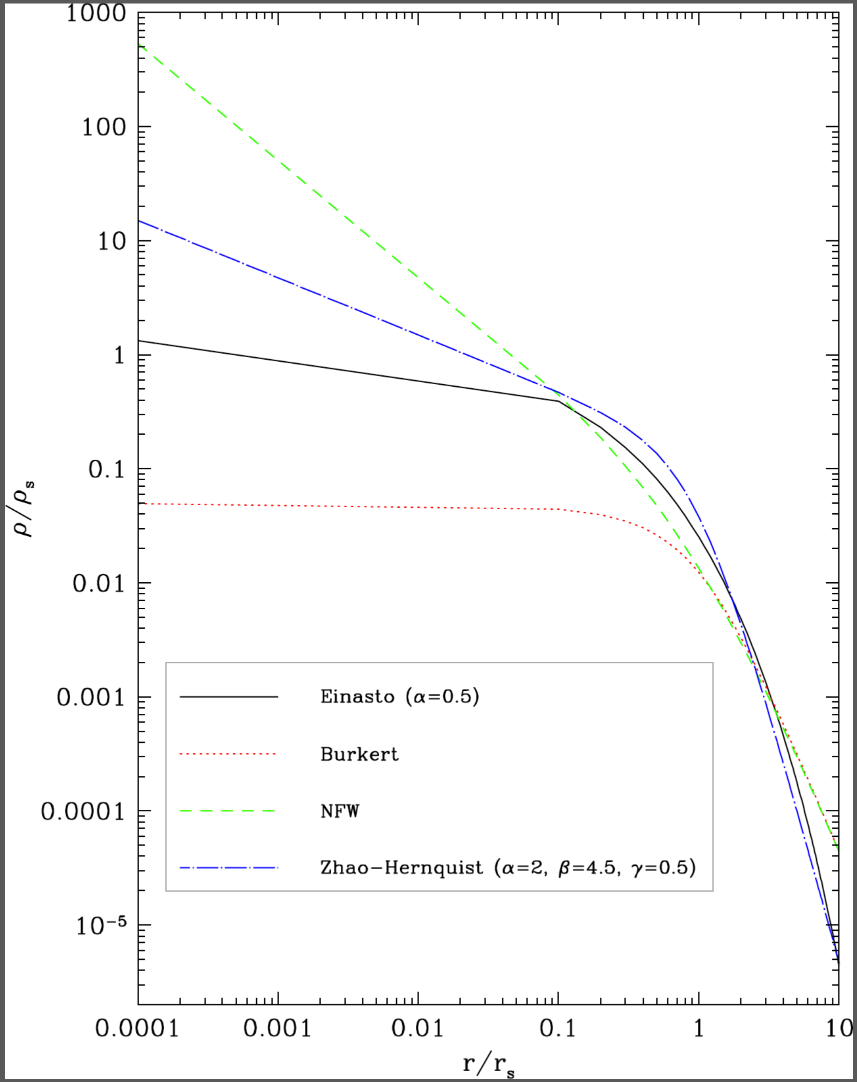

Supplementary material

Mathematical derivation of the 2nd-order Jeans equation:

Liouville equation

$$\frac{\partial f^{(6N)}}{\partial t} + \left\langle \nabla f^{(6N)}, \mathbf{w}^{(6N)} \right\rangle = 0$$

$$\mathbf{w} = \left(\mathbf{v}, -\nabla \phi_{\mathrm{tot}}\right)$$

no collisions

collisionless Boltzmann equation

$$\begin{cases} \dfrac{\partial f}{\partial t} + \left\langle \mathbf{v}, \dfrac{\partial f}{\partial \mathbf{r}} \right\rangle - \left\langle \nabla \phi_{\mathrm{tot}}, \dfrac{\partial f}{\partial \mathbf{v}} \right\rangle = 0 \\ \phi_{\mathrm{tot}} = \phi + \phi_{\mathrm{ext}} \\ \nabla^2 \phi = -4\pi G \displaystyle\int_{\mathbb{R}^3} f d^3\mathbf{v} \end{cases}$$

steady state

Jeans equation (any symmetry)

$$\begin{cases} \dfrac{\partial \rho}{\partial t} + \dfrac{\partial}{\partial x_i}\left(\rho \overline{v}_i\right) = 0 \\ \dfrac{\partial}{\partial t}\left(\rho \overline{v}_i\right) + \dfrac{\partial}{\partial x_j}\left(\rho \overline{v_i v_j}\right) + \rho \dfrac{\partial \phi}{\partial x_i} = 0 \end{cases}$$

spher. symm.
no rot. support

spherical Jeans equation

$$\frac{1}{n_*}\left[\frac{d}{dr}\left(n_* \overline{v_r^2}\right)\right] + \frac{2}{r}\beta_{\mathrm{ani}}(r)\overline{v_r^2} = -\frac{G\left[M_{\mathrm{DM}}(r) + M_*(r)\right]}{r^2}$$

Supplementary material

FIRST CAVEAT: we are dealing with projected quantities (2D instead of 3D) and potential triaxiality.

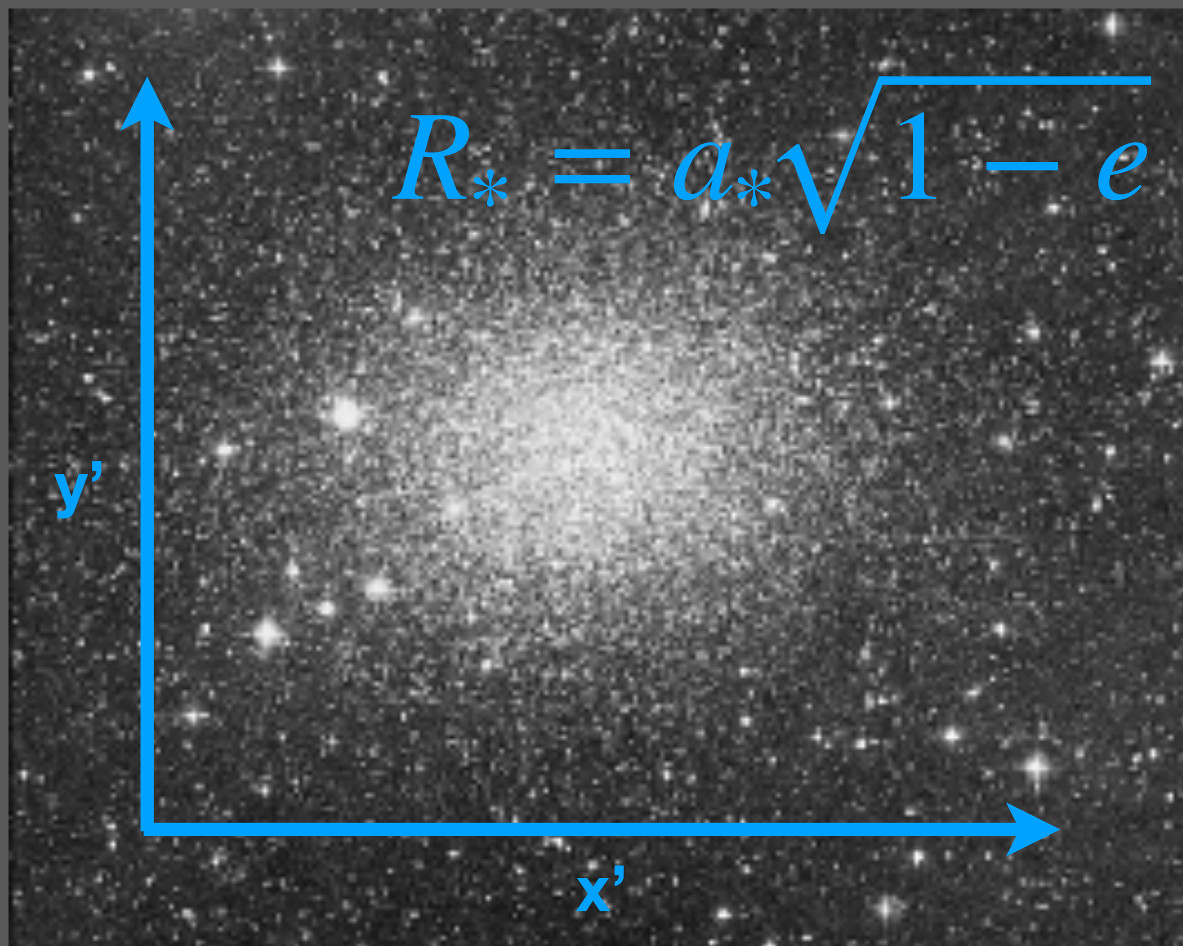

Supplementary material

SECOND CAVEAT: no idea about the tangential velocities of the member stars.

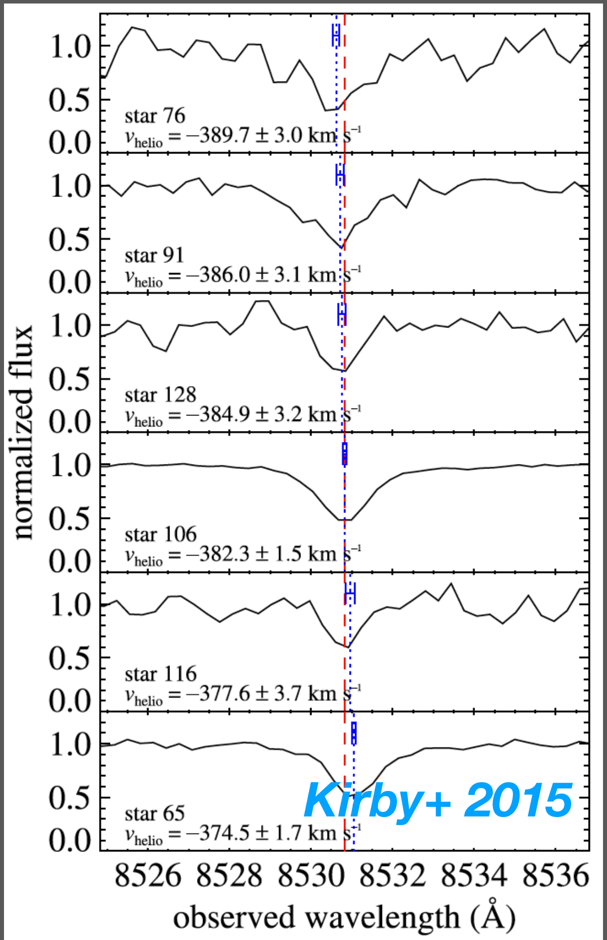

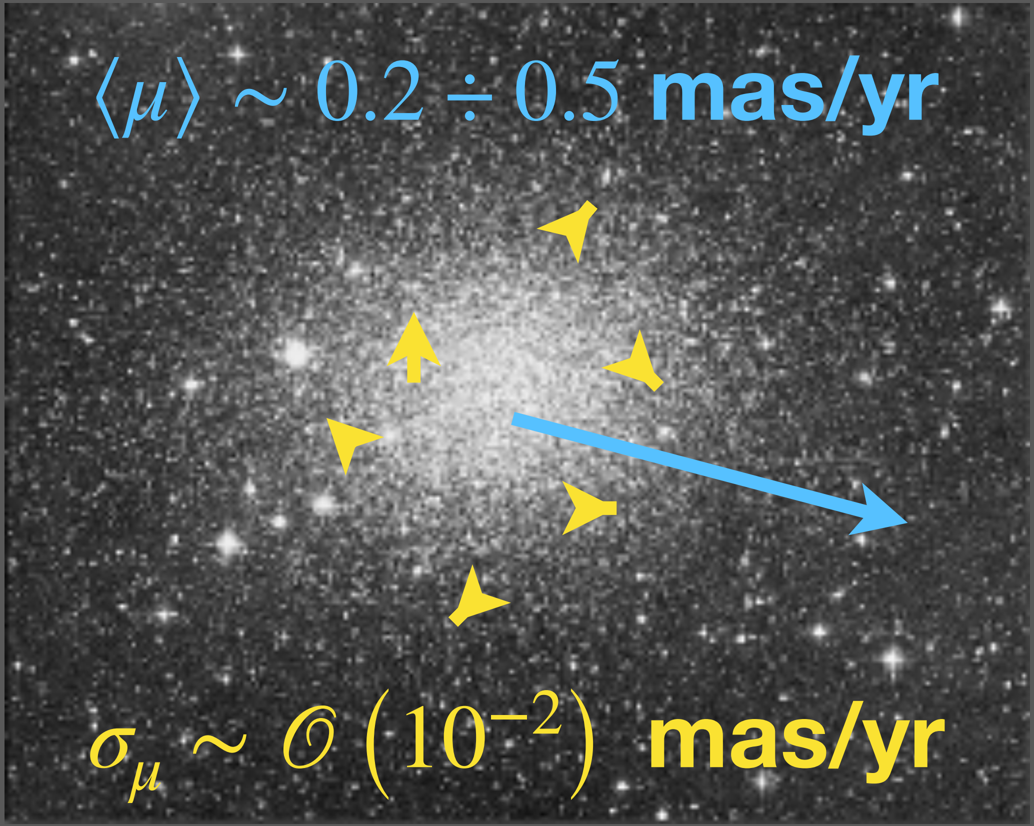

Supplementary material

THIRD CAVEAT: uncertain origin of dSph kinematics (mini-DM halos vs. remnants of tidal disruptions).

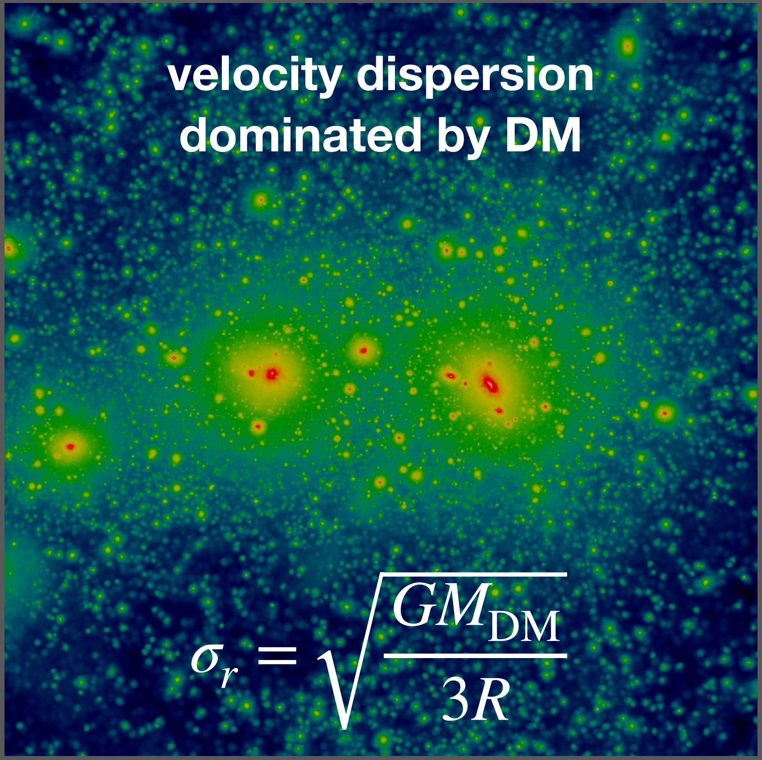

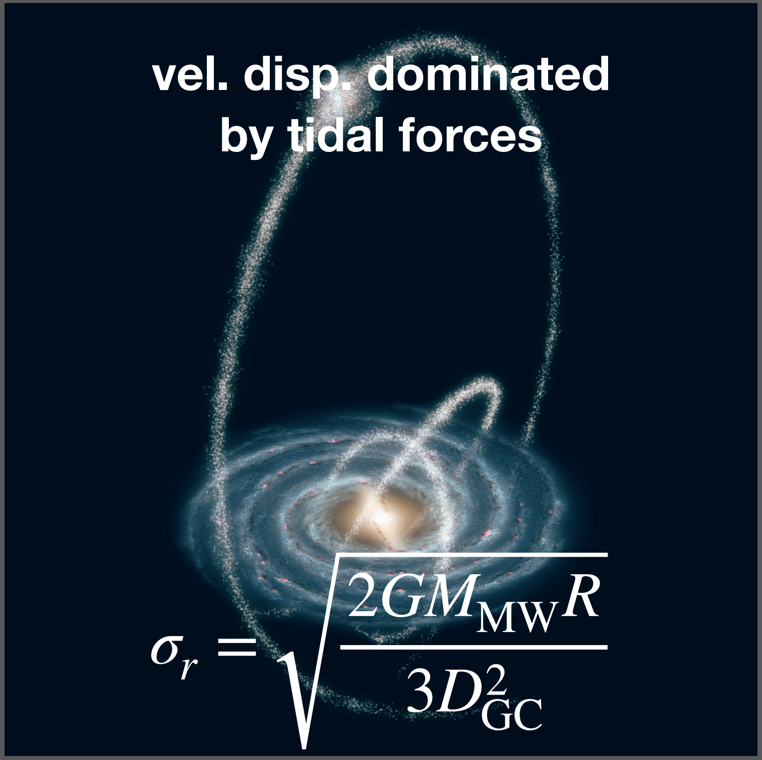

Supplementary material

FOURTH CAVEAT: foreground stellar populations contaminating the member sample.

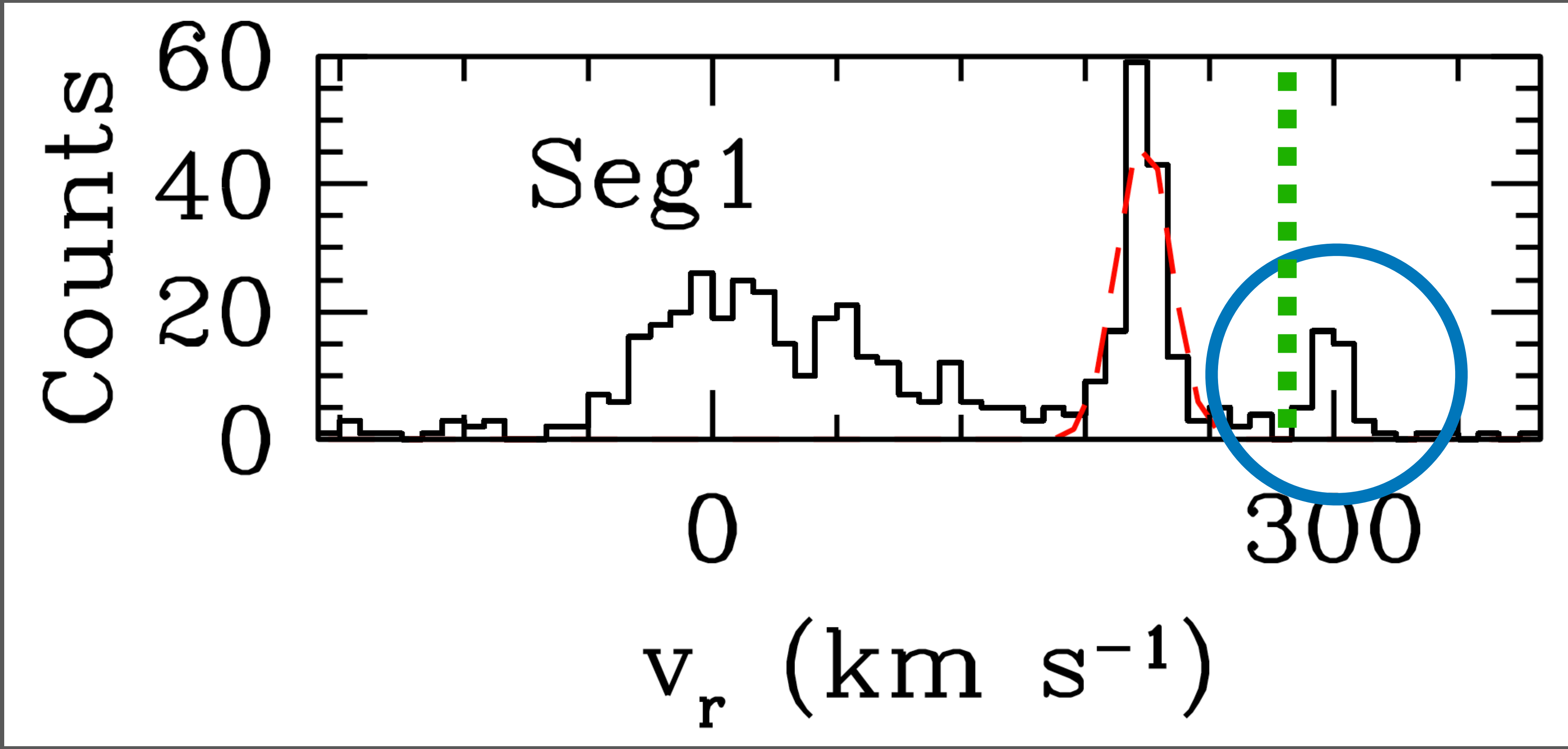

Supplementary material

FIFTH CAVEAT: unreliable stellar samples for objects with small numbers of members.

ID	R (pc)	v_r (km s^{-1})	δv_r (km s^{-1})	Data set
1	1.9	−381.4	1.3	K&M
2	5.0	−380.7	2.4	K&M
3	8.5	−382.1	2.1	K&M
4	10.2	−384.9	3.2	K
5	10.3	−383.1	4.9	M
6	10.7	−389.0	2.3	K&M
7	11.2	−373.8	1.4	K&M
8	19.4	−387.0	3.8	M
9	21.2	−401.4	6.6	M
10	30.3	−362.8	5.6	M
11	31.4	−397.1	7.8	M
12	32.7	−404.7	5.1	M
13	36.8	−387.1	7.7	M
14	80.4	−375.8	3.1	M

ID (K15a)	ID (M16)	R.A. (J2000)	Decl. (J2000)	Radius (arcmin)	$(g_{P1})_0$ (mag)	δg_{P1} (mag)	$(i_{P1})_0$ (mag)	δi_{P1} (mag)	Masks	S/N[a] (Å^{-1})	v_{helio} (km s^{-1})	$\sigma(v)$	Member?
···	22	02 13 12.69	+36 08 49.4	2.11	20.71	0.09	20.34	0.09	cdefg	44.5	−380.6 ± 3.0	0.6	Y
128	···	02 13 14.24	+36 09 51.1	1.06	19.93	0.03	19.41	0.03	bdeg	25.0	−383.3 ± 1.8	0.4	Y
116	21	02 13 15.96	+36 10 15.8	0.53	20.38	0.02	19.92	0.02	bcdeg	26.4	−381.4 ± 3.2	0.9	Y
106	40	02 13 16.55	+36 10 45.8	0.19	17.34	0.01	16.58	0.01	bdef	219.5	−381.6 ± 1.6	0.4	Y
91	20	02 13 19.32	+36 11 33.3	0.93	20.33	0.03	19.79	0.03	bcfg	29.7	−380.1 ± 4.9	1.7	Y
76	23	02 13 20.61	+36 09 46.5	1.12	20.83	0.06	20.53	0.06	bcg	17.0	−385.2 ± 4.2	1.3	Y
···	27	02 13 21.35	+36 08 29.1	2.36	21.30	0.07	21.27	0.07	cd	20.0	−376.8 ± 11.7	1.6	Y
65	46	02 13 21.54	+36 09 57.4	1.11	19.03	0.01	18.42	0.01	bdfg	81.8	−381.0 ± 5.9	3.0	Y
···	24	02 13 22.00	+36 10 25.9	0.97	21.22	0.07	21.14	0.07	d	17.8	−370.4 ± 17.1	···	Y
···	26	02 13 24.83	+36 10 21.8	1.54	21.40	0.11	21.17	0.11	c	19.9	−375.6 ± 11.2	···	Y
···	9	02 13 27.33	+36 13 30.5	3.45	21.25	0.10	21.05	0.10	d	17.6	−387.6 ± 7.7	···	Y
···	29	02 13 30.95	+36 11 56.0	3.00	21.96	0.20	21.68	0.20	c	14.0	−386.2 ± 4.7	···	Y
···	31	02 13 52.66	+36 13 24.1	7.61	20.63	0.03	20.12	0.03	cdg	42.8	−377.1 ± 2.7	0.9	Y
···	25	02 13 17.14	+36 07 14.1	3.47	21.15	0.05	21.07	0.05	cd	21.3	···	···	?[b]

binary star

total sample dimension: 14 stars

revised sample dimension: 13 stars